

RESEARCH ARTICLE

Flexural Strength and Failure Behavior of Glass Laminate Aluminum Reinforced Epoxy and Aluminum-Lithium Laminates in Abrasive Water Jet Peening Under Contamination

Syed Qutaba^{1,3*}, Galang Sandy², Sajjad Ahmed⁴, and Azmir Azhari¹

¹Faculty of Manufacturing and Mechatronics Engineering Technology, Universiti Malaysia Pahang Al-Sultan Abdullah, 26600 Pekan, Pahang, Malaysia

²Faculty of Mechanical and Automotive Engineering Technology, Universiti Malaysia Pahang Al-Sultan Abdullah, 26600 Pekan, Pahang, Malaysia

³Department of Textile Engineering, Balochistan University of Information Technology Engineering & Management Sciences, 87300 Quetta, Balochistan, Pakistan

⁴Faculty of Engineering, University of Larkano, 77150 Larkana, Sindh, Pakistan

ABSTRACT – Abrasive Waterjet Peening (AWJP) technology has been widely utilized for various machining, surface treatment, and material indentation applications. The goal of this study is to investigate the influence of AWJP parameters (stand-off distance, water pressure, abrasive size, and number of passes) on the bending strength and types of damage during the peening process of the Fiber Metal Laminates (FML). The surface treatment with AWJP has resulted in variant effects on the surface of the FML. Furthermore, the effect of FML structure with spreading layers was investigated for deformation during the AWJP process. Analysis of variance (ANOVA) was used in the present study to evaluate the effect of AWJP parameters on the failure behavior of 3/2 aluminum-lithium alloy and glass fiber laminate. Results indicated that the fiber layers hindered the deformation of the aluminum-lithium layer. Moreover, the layup of fiber layers and the abrasive size affected the craters' shape on the metallic surface of aluminum-lithium layers. In terms of four parameters, it was found that the medium level of parameters was sufficient based on ANOVA, which showed a higher flexural strength (up to 482 MPa). Based on the results related to flexural strength, the residual stress field of the FMLs under multiple passes indentation was simulated as the higher flexural strength. The prediction and actual values were consistent with the experimental results, with the overall increase being $\pm 10\%$. "Effect" A morphology study revealed that "FML flexural strength deteriorated and caused damage due to the high impact intensity of peening with increases in the craters effect." Hence, resistance is effective at low impact due to the high craters effect.

ARTICLE HISTORY

Received : 13th May 2024

Revised : 25th Oct. 2024

Accepted : 08th Nov. 2024

Published : 20th Feb. 2025

KEYWORDS

AWJP

Fiber metal laminate

Failure behavior

ANOVA

Machining parameters

1. INTRODUCTION

Abrasive WaterJet Peening (AWJP) is amongst the most rapidly developing and intensely researched methods of surface treatment process [1]–[3]. AWJP employs a jet of water to enhance the speed of the abrasive particles to a level sufficient for effectively processing significantly more rigid materials [4]–[6]. Waterjets can be categorized according to their fluid medium, which includes plain water, water with soluble additives, and water with non-soluble abrasives [7]–[9]. AWJP technology is due to its inherent cold machining properties; this technology is extensively utilized in several industries, such as automotive, medical, and aerospace [10], [11]. AWJP improves surface hardness, roughness, and residual stress, significantly increasing the fatigue life of treated materials like titanium alloys and stainless steel [12], [13]. Abrasive Waterjet (AWJ) is helpful in cutting and surface treatment, cleaning, and coating removal [14]–[16]. Compared to traditional machining methods, cold machining methods such as AWJ do not have heat-affected zones in the cutting area and require minimum force. This is because of the cold machining process's nature [17]–[20]. Since AWJP involves abrasive particles, unwanted material removal is risky, which can alter the dimensional accuracy of the treated surface [21].

Fiber metal laminates, also known as FMLs, are hybrid materials that combine the outstanding deformation resistance and high strength of fiber-reinforced polymer (FRP) composite plies. These plies comprise metal layers and fiber-reinforced composite plies that are alternatively inserted [22]–[24]. Glass Laminate Aluminum Reinforced Epoxy (GLARE) is widely used on A380 fuselages due to its high strength, good fatigue resistance, and impact resistance as exhibited by the second generation of FMLs [25], [26]. The widespread adoption of FMLs in the aviation industry as high-performance materials clearly indicates their value. These materials have been commonly employed in manufacturing fuselages and wings for large aircraft, thus not only emphasizing their significance but also demonstrating their indispensable contribution to advancements in the aviation industry [27], [28]. The integration of GLARE into the top fuselage skin of the Airbus A380 resulted in a remarkable weight reduction of 794 kilograms, showcasing the material's efficiency in improving overall aircraft performance by minimizing weight without compromising structural integrity. Recent findings indicate that FML reduces the contact angle, enhances the surface area of the fibers, and

*CORRESPONDING AUTHOR | Syed Qutaba | ✉ PFI20002@student.umpsa.edu.my

reinforces the roughness of the surface [29], [30]. The adhesive layers have undeniably improved the interlaminar characteristics, strength, and deformation of the FMLs. Composite materials have many applications, such as constructing bridges, manufacturing aircraft fuselages, and producing components for sporting equipment [31], [32].

As evidenced in the previous study, AWJP has held an undeniable advantage over other technologies regarding surface finish and material properties [33], [34]. Alternative material removal and cutting techniques, including electrical discharge machining (EDM), laser cutting, ultrasonic machining, and abrasive waterjet machining (AWJM), have gained considerable interest as unconventional energy sources. The potential and effectiveness of these methods have been thoroughly investigated [35]. However, there is a risk of surface over-peening, leading to micro-cracking, which can compromise the material's integrity. Therefore, controlling the balance between peening intensity and material preservation is crucial; nevertheless, this can be challenging, especially for delicate materials [36]. The presentation of the fibers within the composite plays an essential role in determining the mechanical properties of the material [37]. The fiber affects the composite's strength, stiffness, and failure modes. Generally, fiber's existence provides the highest strength, stiffness, and maximum shear strength. In FMLs, the fiber also affects the bonding between the metal and composite layers [38], [39]. When the fibers are oriented perpendicular to the metal layer, they can form interlocking structures that improve the bonding between the layers and increase the energy absorption capacity of the material [40].

Overall, the fiber's presence in FMLs is a crucial design parameter that can be tailored to achieve specific mechanical properties and optimize the material's performance for specific applications [41]. The fibers in the composites can influence the performance of water jet machining. The effectiveness of a water jet depends on several factors, including the material being cut and the orientation of any fibers in the material [42], [43]. The incorporation of lithium into aluminum results in an increase in modulus and a decrease in density. Compared to ordinary aluminum alloys, alloy 8090 contains lithium. Aluminum is of tremendous importance to the aerospace and aircraft sectors [44], [45]. Before 1980, only a handful of commercial aluminum-lithium alloys were suitable for use in the aerospace industry [46]. The paper is organized as follows: Section 2 has an experimental part which covers the fabrication and machining parameters. Section 3 discusses the analysis data, which covers the ANOVA and responses of the flexural strength, further fractography and characterization of the material involved. Finally, Section 4 concludes the paper by summarizing key findings and suggesting future research directions.

This study examined the effect on the FML properties across the AWJ peening process. For this reason, the work reported here investigates the impact of four different parameters on the composite under the same FML surface and structure. They have been categorized into three levels and selected based on the constant and discrete. In the present research study, the bending strength and failure behavior will be investigated using the design of experiment (DOE) and ANOVA. The results were based on the differentiation in the peening, which was treated using the optimized combination of the parameters. The failure behavior and bending strength have been observed at the universal testing machine (UTM) and under fractography. Traditional surface treatments for FMLs often focus on other methods, such as shot peening or mechanical abrasion. By introducing AWJP to FMLs, it was anticipated that this study would pioneer a new surface treatment approach that could potentially enhance the properties of FMLs.

2. EXPERIMENTAL

2.1 Fabrication of the FML Composite

The process of layering was used to laminate the fiber layers and aluminum-lithium 8090 sheets. Once the sheets were positioned, the epoxy solution was administered between each layer and compressed using hydraulic pressure. The compressed and sprayed composite pieces were placed vertically in a furnace for curing at an initial temperature of 150°C [40]. Figure 1 illustrates the design of the FML used in the present study, while Figure 2 illustrates the stages involved in the preparation of the aluminum-lithium alloy sheet and glass fiber FML composite.

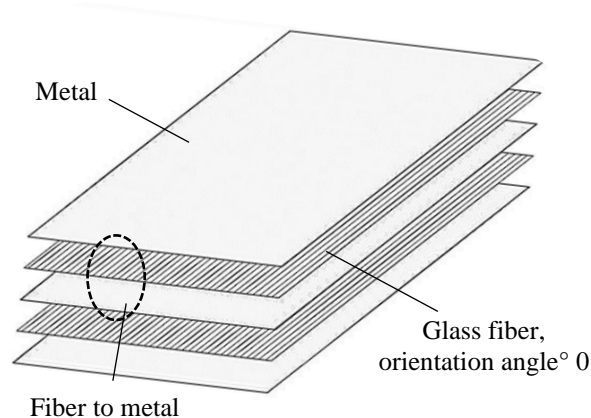


Figure 1. Fiber metal laminate structures with spreading layers

In the second stage of the process, a solution-aging technique was employed to enhance the aluminum-lithium layers, bringing them to the T3 layer condition. This was achieved by performing the solution treatment using a KU-15-06-A air-circulating boiler, meticulously designed to maintain accurate and uniform temperature control. The treatment was conducted at a high temperature of 525 °C for a duration of 30 min, ensuring the reliability and consistency of the procedure for optimal material strengthening. The alloy underwent water quenching, followed by a 2% pre-deformation and natural aging at room temperature, resulting in the attainment of the T3 state. The aluminum-lithium layers underwent a specialized surface treatment process to improve the bonding capabilities with fiber-reinforced composites. This treatment required phosphoric acid anodizing, a method specifically chosen to enhance surface properties and promote stronger adhesion between the layers and the composite material. This process involved using a solution of phosphoric acid (H₃PO₄) with a concentration of 150 g/ml at a temperature of 20 °C, applying a voltage of 15 V, and allowing the treatment to proceed for 15 minutes. The primary objective of this treatment was to generate a textured surface on the aluminum-lithium layers, enhancing the compatibility of these layers with other materials. Following this, the lamination process was carried out using a combination of an autoclave and hydraulic pressure, which facilitated the precise bonding of aluminum sheets with glass fiber layers to form a durable and integrated composite structure.

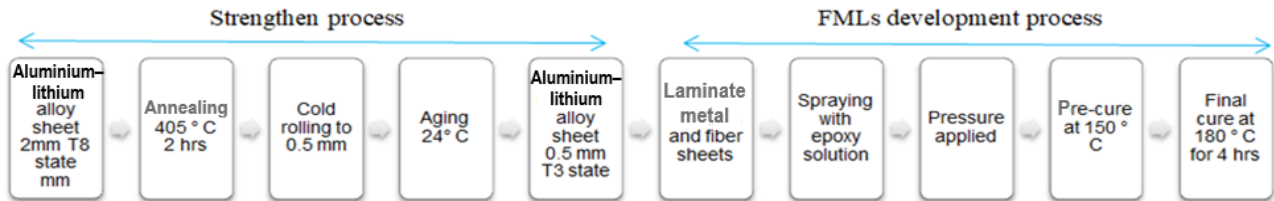


Figure 2. Preparation process of an aluminum-lithium alloy sheet involves the development stages of a laminate composite fiber metal

An aluminum-lithium alloy and a glass fiber sheet were utilized to conduct the research investigation. An epoxy system made of resin and hardener was fabricated for the FML. A 2:1 ratio was used in this process. After the sheets were installed, the gaps between them were filled with an epoxy solution to ensure complete bonding. During the process, the assembly was subjected to hydraulic pressure of approximately 0.68 MPa to enhance adhesion and eliminate voids. Initially, the composite components, which had been pressed and coated with the epoxy, were heated to a temperature of 150 °C. This preheating step prepared the materials for the subsequent curing fixation process, which was conducted in a furnace to ensure structural stability and strength [40]. The dimension of the sample composite used for analysis is equal to bending strength, around 8 cm long and 3 cm in width with 2 mm thickness.

2.2 Equipment

The experiment used a commercial low-pressure waterjet peening machine, as illustrated in Figure 3. The system utilized an air-powered hydraulic pump capable of generating water pressure of up to 150 MPa. The motion of the nozzle was controlled in three-dimensional dimensions using a computer numerical control (CNC) system.

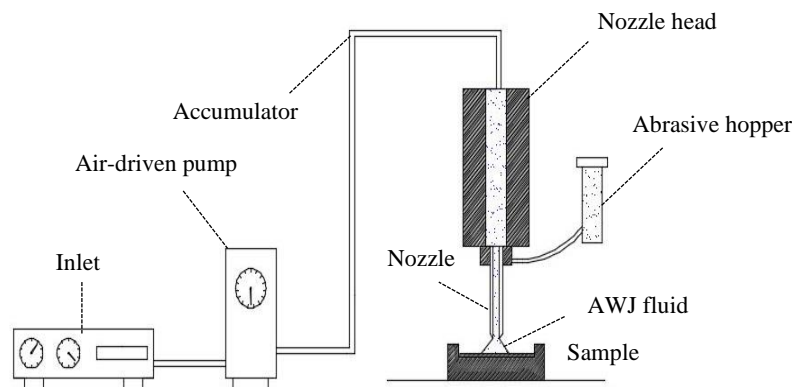


Figure 3. Illustration of AWJ peening

As presented in Table 1, the parameters were selected based on a thorough evaluation of relevant papers on the use of AWJ machining for stainless steel [47]. The constant process parameters are shown in Table 1.

Table 1. Constant machine parameters and their values

Constant parameters	Value
Orifice diameter	0.127 mm
Focusing tube diameter	0.762 mm
Abrasive type	GMT garnet
Abrasive-mass flow rate (g/min)	9

2.3 Experimental Design

The current study examined four peening parameters (see Table 2). The values of selected levels were determined based on a literature review and preliminary experiments. For example, during an initial investigation at low water pressure below 67 MPa, it was found that this did not cause any effect on the FML surface. Further, no changes were received from the treatment; therefore, a pressure of more than 67 MPa would need to be applied.

Table 2. Machining parameters and their levels

Machining parameters	Levels			Units
	1	2	3	
	Low	Medium	High	
Pressure (p)	69	97	117	MPa
Abrasive size (a)	80	120	160	Mesh
Stand-off distance (d)	20	40	60	mm
Passes (n)	1		2	-

By contrast, high pressure above 117 MPa caused severe damage to the FML surface. It is important to note that the experimental design followed a complete factorial approach, with three parameters having three levels each and one parameter having one level. This resulted in a total of 54 combinations or experiments, which were conducted on both ends of the surface. The workpiece was manufactured by sectioning commercially obtainable aluminum alloy 8090 sheet metals. The FML had an approximate thickness of 2 mm. In every test, the orifice diameter and impact angle were maintained at a constant value of 0.127 mm and 90°, respectively. Figure 4(a) illustrates the experimental setup for AWJ peening using the manufactured composite laminate. Each test ran as described in the L54 orthogonal array, and the test was conducted on both sides of the laminates for a length of 30 mm. The nozzle diameter was fixed at 0.127 mm, and the constant traverse rate was 1000 mm/min. The specimen was generally a rectangular bar measuring at least 80 mm in length and at least 10 mm in width. Depending on the substance under examination, its thickness should fall within the range of 2 mm to 10 mm (Standard & ISO, 2019). The test specimen is placed horizontally on two "span supports," separated by a defined distance, as shown in Figure 4 (a).

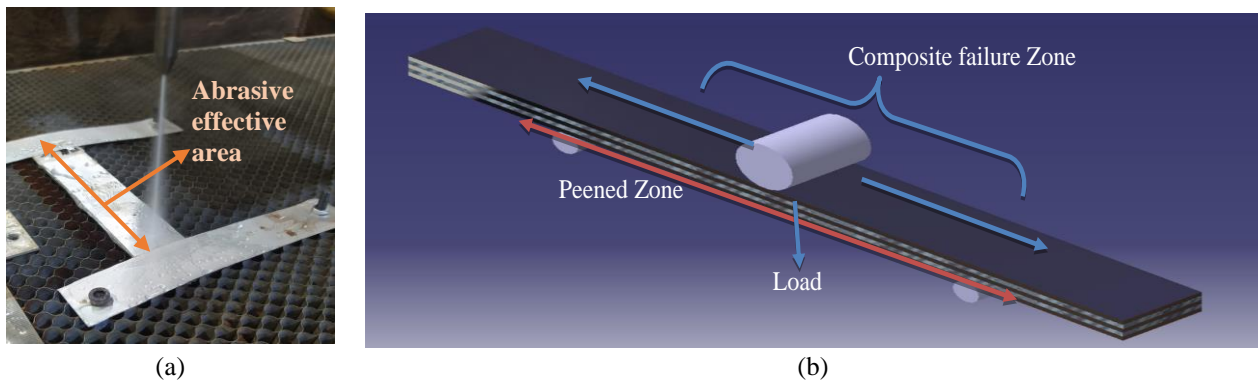


Figure 4. (a) Experimental setup view of AWJ peening, (b) Demonstration of the 3-point bending test flexural strength

The distance between the supports would depend on the thickness of the specimen, as specified in the ISO 178 standard (Organization, 2011). A load was then applied to the center of the specimen by a loading nose, which was attached to a movable crosshead that moved downward at a constant speed. The test was conducted at a specified temperature and humidity per the ISO 178 standard (Standard & ISO, 2019). The load was applied to the specimen until it reached a maximum load or until it would fracture. During the test, the deflection of the specimen was measured using a displacement transducer, and the load was measured using a load cell. From the load-deflection curve obtained during the test, several parameters were able to be calculated to describe the flexural properties of the material, as shown in Figure 4 (b). The most used parameters were the flexural modulus, flexural strength, and flexural strain at the maximum load.

3. RESULTS AND DISCUSSION

3.1 Surface Characterization of the Material

Detailed surface imaging was performed using scanning electron microscopy (SEM) at Universiti Malaysia Pahang Al-Sultan Abdullah (UMPSA) Center's advanced characterization laboratory. This technique was employed to thoroughly observe and analyze the surface features and quality of the materials processed through abrasive water jet (AWJ) machining so that a deeper understanding of the machining outcomes and surface characteristics would be gained. The image processing microscope was used to monitor the cutting edges while cutting. The analysis was conducted to assess micro phenomena that occurred at various parameters. The SEM images, as shown in Figure 5 morphologies, were observed at the top and bottom regions, respectively.

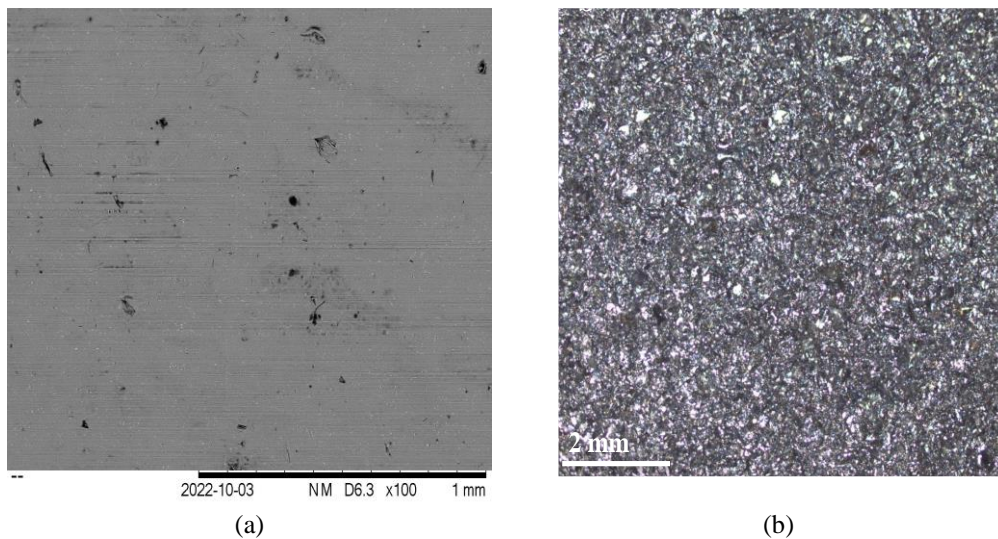


Figure 5. Surface morphology of FML, (a) top region of the unpeened composite, (b) bottom region of the treated composite

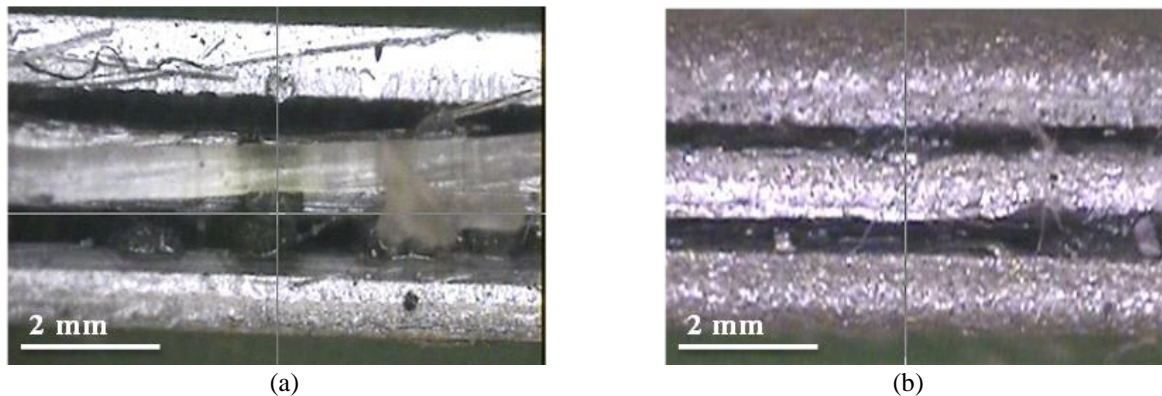


Figure 6. Surface morphology of FML structural, (a) unpeened structure, (b) abrasive collide structure

The fractography was observed through scanning electron microscopy and images micro measurement scope, as shown in Figure 6. The stresses generated during the indentation process demonstrate the obstructive influence of the fiber layers. These stresses also affect the failure characteristics of GFRP/Al-Li laminates. FMLs would be susceptible to failure if they were subjected to excessive indentation stresses.

3.2 Analysis of Variance (ANOVA)

Using analysis of variance (ANOVA) may determine how much each factor would contribute to the differences in the outcome. This would lead to a better understanding of the overall variation and observation of the outcome. The ANOVA results presented in Table 3 include additional calculations based on the initial sum of values. The formulas for calculating the sum of square (SS), variance (V), F-ratio (F), percentage contribution (P) and degree of freedom (df) are given in, respectively. The F-ratio, or the variance ratio, is the ratio between the control factor effect variance (the mean square due to a controlling factor) and the experimental error variance (the mean square due to experimental error). The F-value, which is a ratio calculated in ANOVA, helps to determine if the effects of a factor are significant. Table 3 shows the ANOVA table for flexural strength. Based on the p -value, material and pressure were significant as the p -value was less than 0.05. Material had the highest degree of substantial, followed by factors P (pressure), a (abrasive Size), d (stand-off distance), and n (Number of passes), which were significant and had a low degree of significance on the flexural strength as the p -value was more than 0.05. Based on these results, it would be worth noting that the experimental level pressure was higher than 482 MPa. This correlated with the contribution of the factor material of 74.14%. The factor P (Pressure) and a (abrasive size) have shown greater contribution, and compared to other previous studies, it was found that stand-off distance was the most significant factor at 32.98%, followed by abrasive size in influencing the flexural strength during the abrasive waterjet peening of transformation-induced plasticity (TRIP) metal sheets.

Table 3. ANOVA results of the flexural strength

Control factors	SS	df	Mean square	F-value	p-value	
model	37669.24	9	4185.47	9.49	< 0.0001	Significant
<i>P-P</i>	141.80	1	141.80	0.8215	0.5737	
<i>a-a</i>	6602.89	1	6602.89	14.97	0.0004	
<i>d-d</i>	1861.94	1	1861.94	4.22	0.0462	
<i>n-n</i>	1287.23	1	1287.23	2.03	0.0435	
<i>Pa</i>	1422.67	1	1422.67	3.23	0.0797	
<i>Pd</i>	524.06	1	524.06	1.19	0.2819	
<i>ad</i>	2594.23	1	2594.23	5.88	0.0197	
<i>Pn</i>	432.95	1	432.95	2.96	0.0234	
<i>an</i>	1546.07	1	1546.07	3.74	0.0345	
<i>dn</i>	374.67	1	374.67	1.29	0.3189	
<i>P²</i>	19185.60	1	19185.60	43.49	< 0.0001	
<i>a²</i>	2349.98	1	2349.98	5.33	0.0260	
<i>d²</i>	250.06	1	250.06	0.5669	0.4557	
<i>n²</i>	234.56	1	234.56	1.12	0.3123	
Residual	18526.47	42	441.11			
Lack of Fit	17483.34	16	1092.71	27.24	< 0.0001	Significant
Error	1043.13	26	40.12			
Total	57195.71	56				

3.2.1 Effect of water pressures on FML surface with respect to stand-off distance

The hydraulic pressure has revealed the main effect on different properties of FML surface and structural properties. In comparison, the 3-point bending strengths were analyzed after being normalized relative to the weight and width of the test coupons. This normalization process would ensure a fair evaluation by accounting for variations in the sample dimensions, providing a standardized measure of bending performance. The parameters of the AWJP would give specific strength, and the particular attribution would show an ascending trend with the increase in the strength of the parameters. The pressure had three stages: lower, middle, and high. In Figure 7, it can be seen that pressure primarily impacts the flexural strength of the FML composite in the low to medium range. As illustrated in Figure 7 (b), high pressure would not play a significant role in flexural strength. By consistently enhancing low pressure such as increasing the stand-off distance and abrasive size, the properties of the FML composite would be improved.

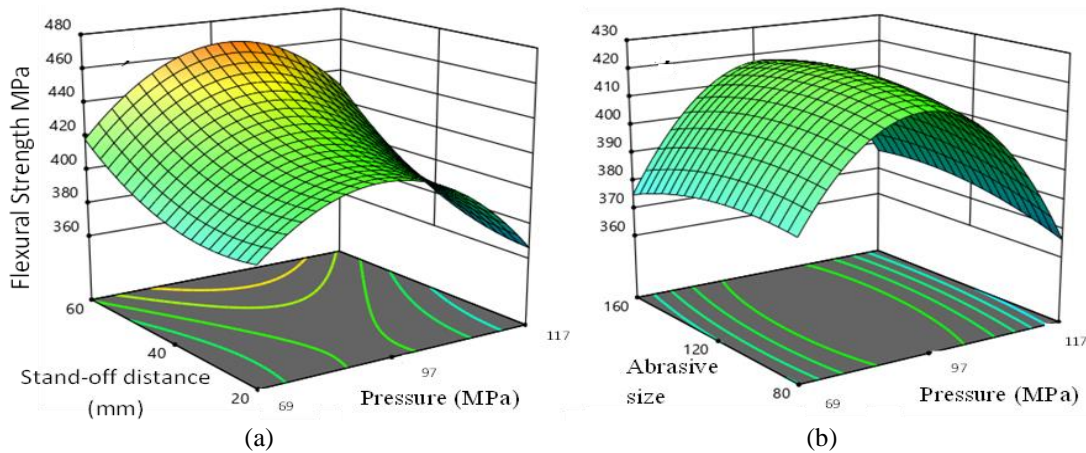


Figure 7. Graphical view of water pressure interacts with different size process parameters, (a) stand-off distance, (b) effect of abrasive size

Figure 8 illustrates a clear trend of decreasing flexural strength with increasing stand-off distance. When the distance increases, the size of the jet diameter increases. As a result, the jet would start to diverge, losing its coherence, thereby reducing the adequate kinetic energy needed. However, in the research, the increase in stand-off distance would reduce erosion when the water temperature was at maximum degree (see Figure 8). This may be attributed to the thinner thickness of the study workpiece. As the abrasive particle would destroy the surface on the upper part section, sliding erosion would occur on the lower part section, producing a smoother texture. Therefore, in such cases, the increase in stand-off distance may allow sliding erosion to occur, reducing the materials' surface roughness. Apart from that, increased stand-off

distance would increase the number of burrs and spurs due to the increased size of a jet plum. Therefore, careful consideration would need to be taken before manipulating the stand-off distance. As shown in Figure 8 (a), the stand-off distance and size of the abrasive have increased the surface energy and reduced the depth of length at the material inside and outside. Figure 8 (b) shows the treated middle stage of pressure, which would primarily affect the flexural strength if the stand-off distance and abrasive size were constant. From Figure 8 (c), it may be understood that, while the constant of both the parameters would still be increasing under very high water pressure, the flexural strength would not increase nor be affected. Furthermore, the flexural strength would be reduced to the original un-peened samples.

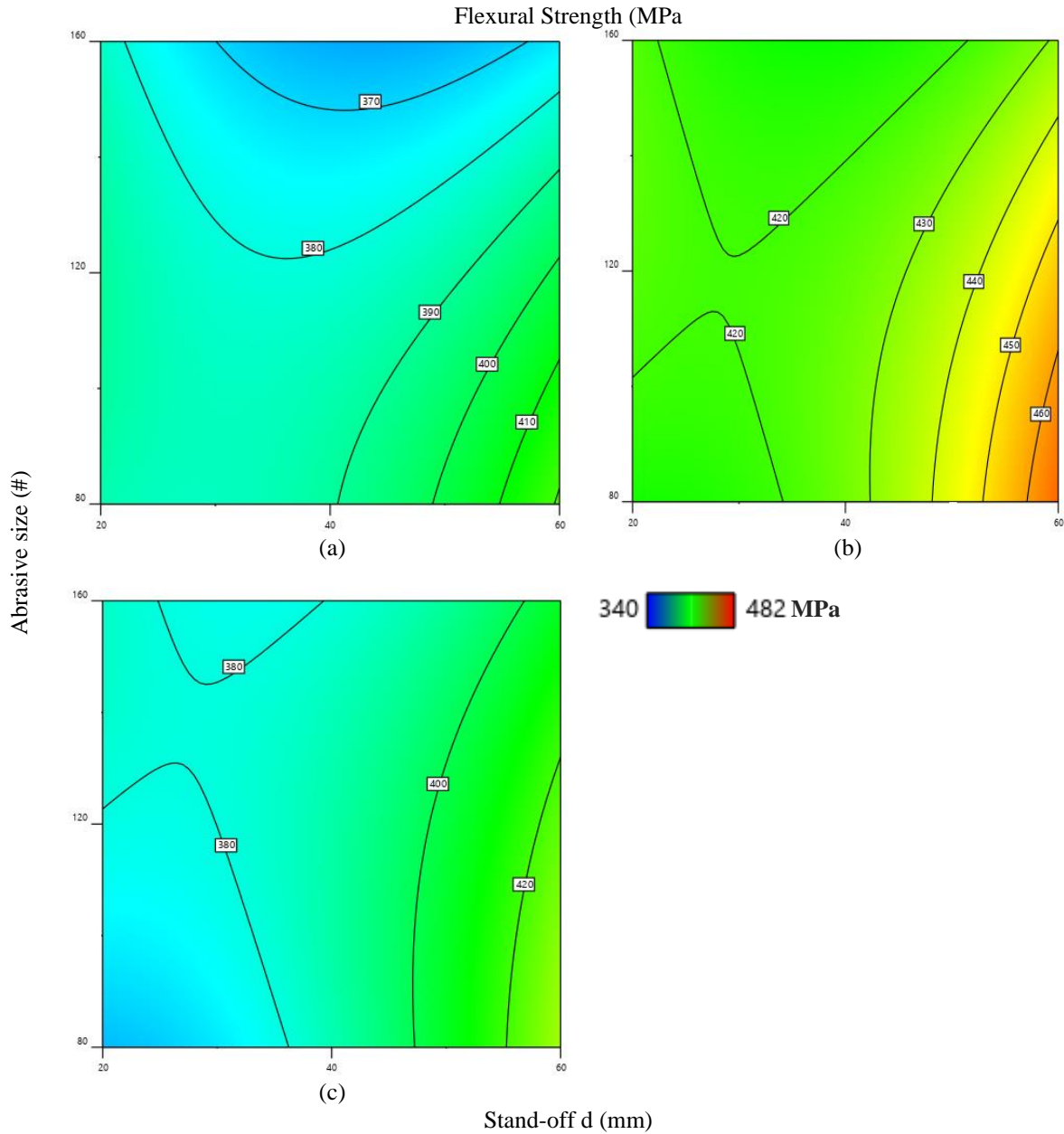


Figure 8. Relationship between stand-off distance and abrasive size effect on flexural strength at different pressures, (a) 69 MPa, (b) 97 MPa, (c) 117 MPa

3.2.2 Effect of abrasive size on FML surface with respect to stand-off distance

The influence of abrasive particle size on the flexural properties of FML is illustrated in Figure 9. The 3D graphical views show that increased abrasive size results in a noticeable decline in flexural strength. This trend highlights the significant role of abrasive size in determining the material's mechanical performance. This is because the further the distance, the bigger the jet diameter would increase the jet's kinetic energy. The 3D graphical views in Figure 9 show flexural strength performance considering two input factors. First, the interaction with the process mesh size and stand-off distance, and second, the water pressure. Figure 9 (a) indicates that the flexural strength could be lower with a large mesh size because less kinetic energy would affect the FML surface.

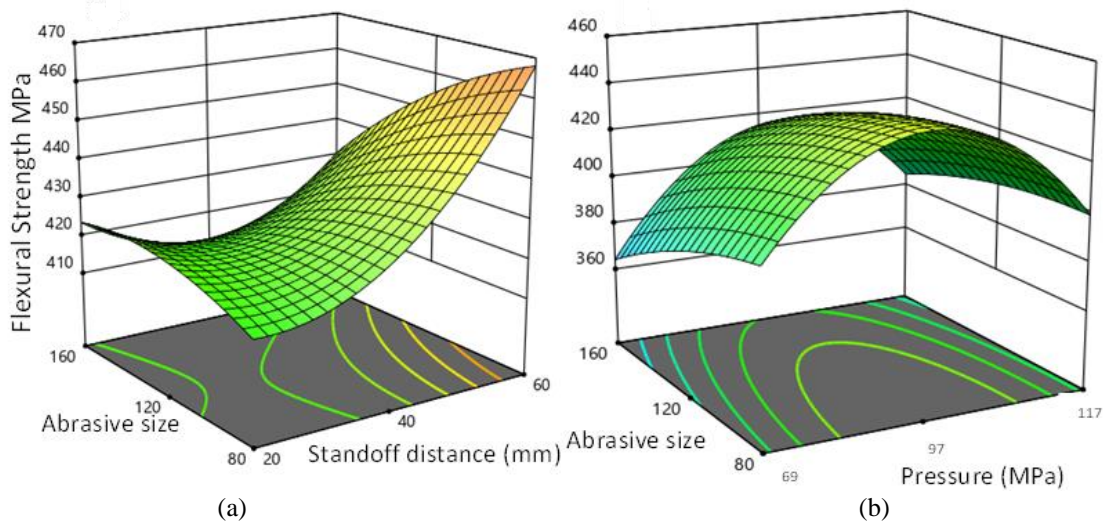


Figure 9. 3D graphical view of abrasive size interacts with different process parameters on flexural strength, (a) stand-off distance, (b) water pressure

Further, it has been revealed that a higher stand-off distance with the lower mesh size would have an impact on the increase in the flexural strength of the FML composite. It has been noticed that the high pressure of water did not affect the properties of the FML, even with the high stand-off distance and mesh size. Based on Figure 9 (b), it was confirmed that the pressure had interacted with mesh size (#) and noticed that low pressure of water affected the surface properties of the FML, resulting in the medium range of flexural strength with the value of 400 MPa. Additionally, it was found that a higher mesh size would generate lower kinetic energy for the jet while interacting with higher water pressure. Thus, the strength value would decline, as shown in Figure 9 (b), with a value of 370 MPa. The curves indicate that adding fibers would result in the ability to withstand higher loads with less pressure than the others. The FML curve has seen an increased load, demonstrating the materials' notable resistance, around 482 MPa, as depicted in Figure 9. The FML curve shows the specimen's gradual transition from elastic to plastic behavior. However, the rate of decrease was quite pronounced, resulting in an abrupt decline. While FML has been widely recognized for its high strength, the observed failure may be attributed to the inherent brittleness of the specimen, which could be further exacerbated by the presence of filler material. The FML curve exhibits increased displacement due to inadequate bonding, indicating that the pre-treatment of the metal was insufficient to facilitate bonding under higher stresses.

Consequently, the material has faced and experienced delamination at lower loads. As it moved to the interaction of different factors related to flexural strength, pressure would act as a primary abrasive measure. Figure 10 shows the main concern of the elements.

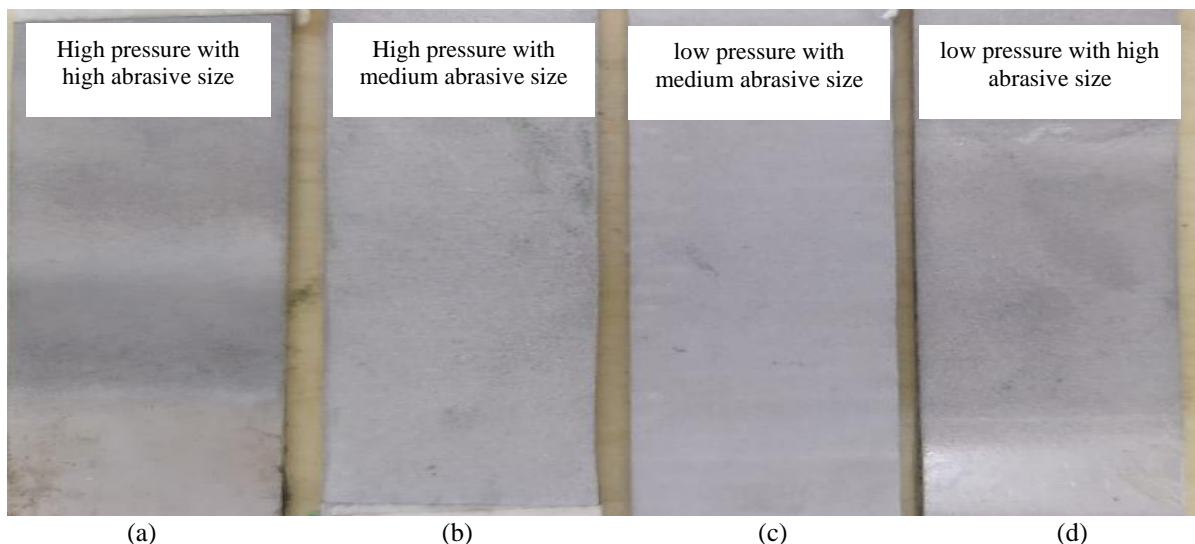


Figure 10. Effect of AWJ peening at surface texture of the FML composite, (a) $P = 117$ MPa, $a = 80$, (b) $P = 117$ MPa, $a = 120$, (c) $P = 69$ MPa, $a = 120$, (d) $P = 69$ MPa, $a = 160$

This research has delved into the influence of variations in jet pressure, the speed at which the nozzle traverses, and the distance between the nozzle and the target surface, focusing on their effects on critical metrics related to surface integrity. The FML composite structures underwent the peening phenomenon under various parametric settings. The study has revealed a notable enhancement in multiple aspects, including structure and surface assessments. Furthermore, the peened

regions' composite surface was examined using microstructural analysis utilizing confocal laser microscopy, as depicted in Figure 10 (a) and (b). The findings of this study have confirmed that significant alterations in the parameters associated with surface integrity may be effectively attained by strategically adjusting critical factors, including the jet pressure, the distance between the nozzle and the surface, and the speed at which the nozzle would move across the material. These modifications may improve the component's performance. The creation of water clusters would induce a cyclic impact phenomenon, resulting in enhanced structural integrity of the surface due to surface deformations. The deformations resulted in compressive residual stresses and were observed in several crystalline defects, including vacancies, dislocations, and twinning. When the pressure was $P = 69$ MPa, the movement of the cylindrical waveguide was hindered within the chamber, preventing the creation of distinct clusters. The hardness variation along the sub-surface of the treated region (depth) is shown in Figure 10 (c), indicating pressure levels ranging from $P = 69$ MPa to $P = 117$ MPa for each abrasive size, as shown in Figure 10 (d).

3.3 AWJP Coverage Changes at Structural and Fractography Changes of the FML

The findings of the present study have indicated a positive correlation between maximal hardness and the increase in stand-off distance. The observed behavior may be attributed to the distinct characteristics of the jet formed at the stand-off distance. The increased distance between the jet and the target amplified the pulse amplitude. This amplified effect ultimately led to elastic-plastic deformations, which occurred within both the surface and sub-surface layers of the material. These deformations arose due to repeated mechanical contact, a phenomenon commonly referred to as the hammer effect.

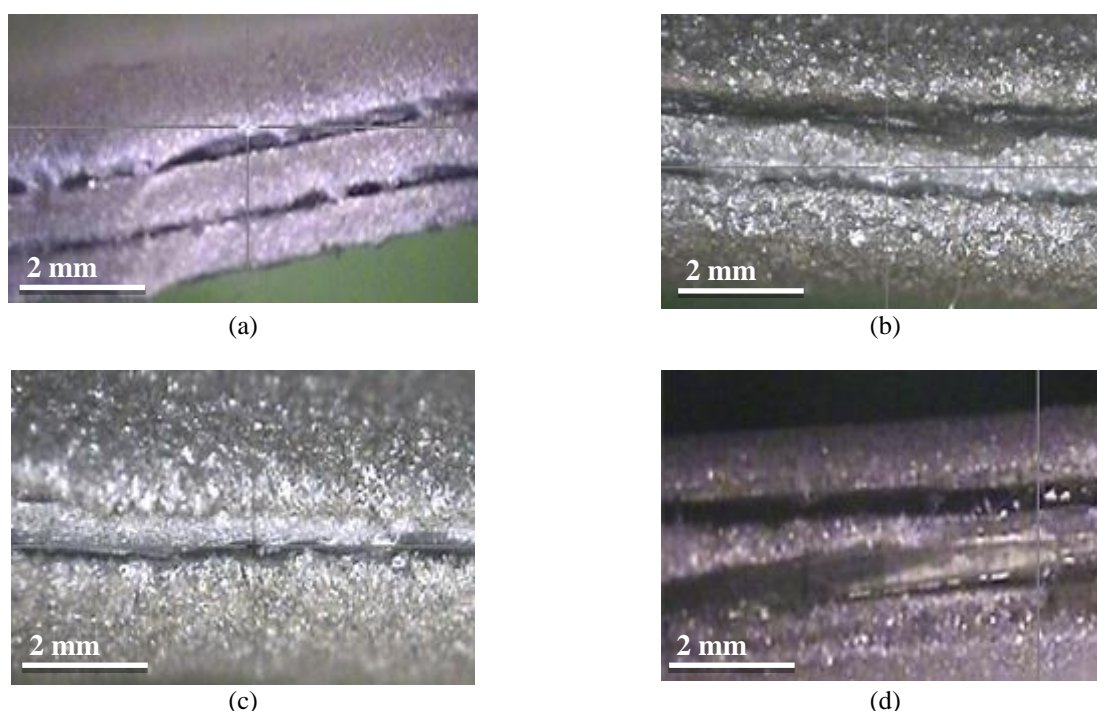


Figure 11. Surface fractography of the FML composite with variation in AWJP factors, (a) Two passes with low impact, (b) Single passes with low impact, (c) Two passes with high impact, (d) Single passes with high impact

Plastic deformation of the material occurred, displacing dislocations and subsequent work hardening of the surface layers. Consequently, the peened surfaces induced plastic deformation within the treated region, resulting in modifications to the characteristics across the depth. The highest work hardening rate was observed in the layers closest to the surface. In addition, it can be seen, as shown in Figure 11 (a), that the application of lower impact with two passes enhanced the maximum surface texture. The obtained outcome followed the measures of surface roughness and grain. The observed behavior of the cover may be attributed to the specific properties of the jet created under varying pressure settings, specifically low impact with single passes and higher impact with two passes, with varied parameter conditions, as shown in Figure 11 (a) and (b), respectively. The creation of discrete water clusters was observed at a lower impact, as opposed to a more significant pressure of high impact, as shown in Figure 11 (c). This phenomenon led to peened pits and the subsequent strengthening of the surface layers. The maximum hardness decreased as the stand-off distances of the nozzle increased from 20 mm to 60 mm. The variation observed in the hardness values was primarily attributed to the duration of exposure time allotted for the jet to engage with and impact the target surface. This interaction time played a crucial role in determining the extent of the changes in hardness. The metal layers and pre-preg layers exhibited a state of continuity and preservation. There was no evidence of visible delamination or microcracks from AWJP, as shown in Figure 11 (d).

The results of the stress tests are presented in Table 4, which provides evidence of the enhanced flexural strength following the AWJP procedure. Applying compressive stress could hinder the formation of cracks on the surface, thus

improving the metal layer's physical characteristics. While the fibers would bear most of the load in FML, a break in the metal could lead to stress concentration, as shown in Figure 11. Hence, generating cracks in the surface metal layers during AWJP would be challenging, ultimately leading to enhanced mechanical properties of the aluminum alloy. Furthermore, it may be inferred that the integrity of the interfacial bonding in the FMLs would remain intact following AWJP using the specified parameters. This is because interfacial adhesion would play a crucial role in facilitating the passage of stress from the surface of the FML to the load-bearing fibers.

Table 4. Effect of AWJP parameters level at the stress and strain

Pressure (MPa)	Abrasive Size (<i>a</i>)	SOD [mm]	Maximum Force [KN]	Maximum Stress [MPa]	Maximum Strain [%]	Flexure strain (Displacement) gauge length
69	80	20	3811.58	389.16	5.5	833.33
69	160	60	3801.58	385.28	5.5	833.33
97	80	20	4501.58	453.56	3.8	833.33
97	160	60	4671.83	467.89	3.8	833.33
117	80	20	4022.16	402.14	3.5	833.33
117	160	60	3991.16	399.17	3.5	833.33

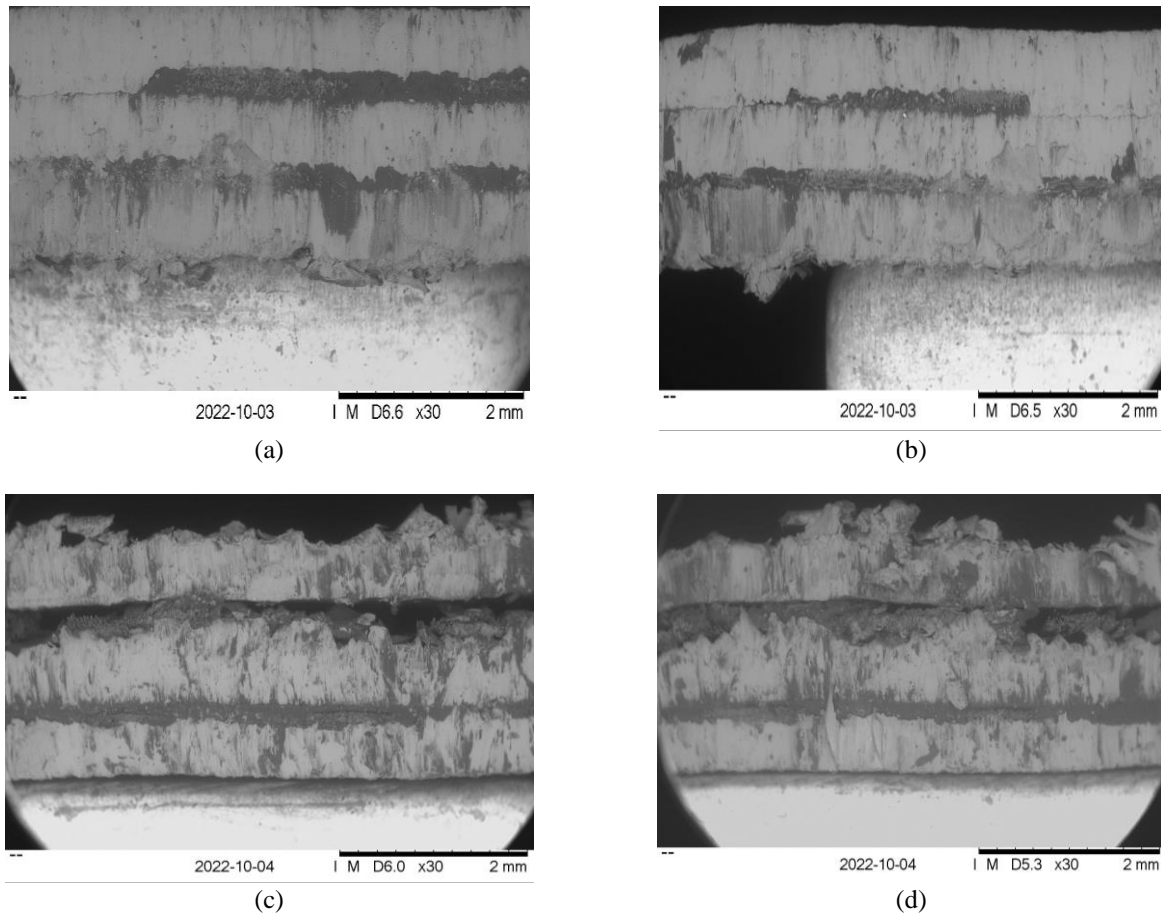


Figure 12. SEM images of FML composite cross-section fractography study with different parameters, (a) $P = 69$ MPa, $a = 160$, $d = 60$ mm, $n = 1$, (b) $P = 97$ MPa, $a = 120$, $d = 40$ mm, $n = 1$, (c) $P = 117$ MPa, $n = 80$, $d = 40$ mm, $n = 2$, (d) $P = 117$ MPa, $a = 80$, $d = 20$ mm, $n = 2$

The deformation behavior of the material under study was significantly influenced by its microstructure. The investigations effectively showed that the structural modifications occurring in the surface layer of materials would only harden using the ultrasonic impact peening method (UIP) without any reinforcement. Figure 12 (a) shows that the surface layer and pre-pegs underwent significant deformation due to the repeated strikes of high-energy pins. This phenomenon resulted in a significant reduction in dislocation density and subsequent reorganization of dislocation structures. This reorganization included the development of dislocation cell structures and the gradual refinement of sub-grains and grains.

Furthermore, it was observed, as shown in Figure 12 (b), that the application of solid plastic deformation resulted in the generation of significant compressive residual stresses. The observed structural characteristics were a direct

consequence of the cold working process, leading to a notable increase in the hardness of the material treated with UIP. The distribution of the parameters has been categorized with the parameters coded as "low to medium" and "medium to high." Furthermore, it is worth noting that the observed microstructural changes were characterized by a notable increase in line broadening, as visually illustrated in Figure 12 (c) and (d).

3.4 Abrasive Waterjet Peening Impact at the Flexural Strength of Fiber Metal Laminates

In contrast to when the coupons' weight and width normalize the 3-point bending strengths, the AWJP parameters exhibited specific strength, and the particular attribution showed an ascending trend as the strength parameters increased, as illustrated in Figure 13. The observed enhancement in particular strength may be attributed to the reduction when the corrugation angle decreased in both the weight and width of the corrugation unit cell, as shown in Figure 13 (a). Figures 13 (a) and (b) provide a detailed depiction of how changes in the thickness of the core sheet influence two critical mechanical properties: shear strength and specific bending strength. The illustrations effectively highlight the relationship between varying core sheet thicknesses and their corresponding impacts on these strengths for a consistent corrugation angle of 45°.

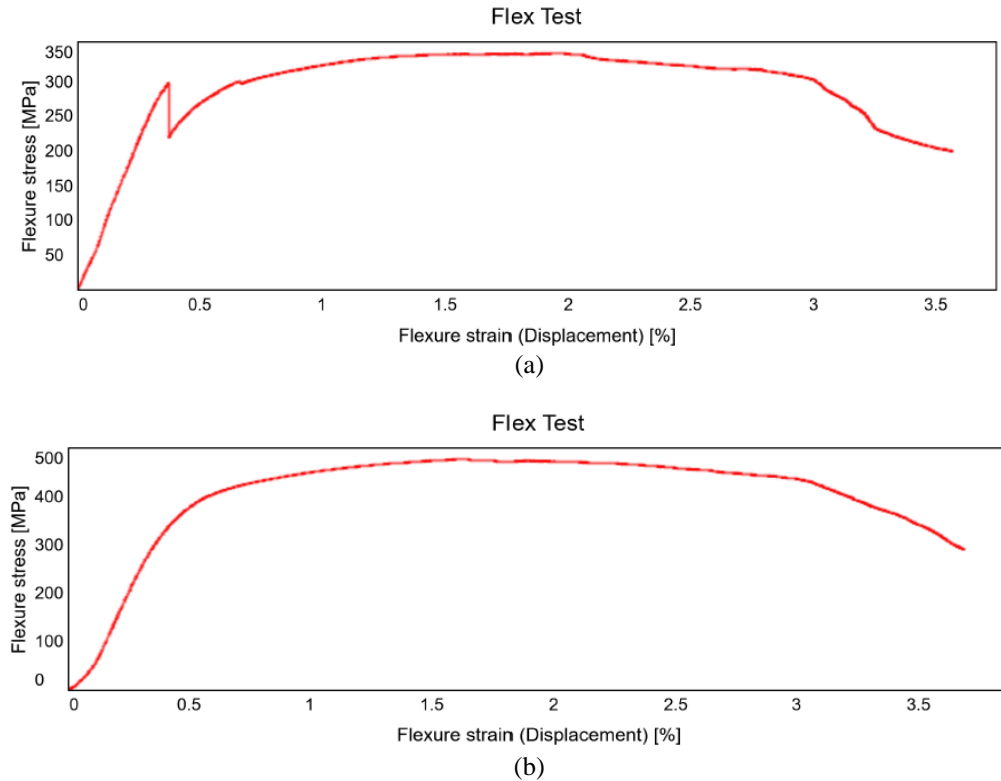


Figure 13. Bending strength enhanced through AWJ peening, (a) un-treatment composite strength, (b) AWJ peened composite strength ($P = 97 \text{ MPa}$, $d = 60 \text{ mm}$)

The results have indicated that the bending strength of the sample increased in direct proportion to the treatment applied. The abrasive size increased from (#) 80 to 120, thus increasing the bending strength, as shown in Figure 13 (b). Nevertheless, as the strength increased, the size of the abrasive decreased, thereby affecting the pressure-induced bending failure modes. The area of maximum pressure, situated at the central part of the upper surface in contact with the specimen, exhibited the most significant damage. The damaged region expanded as the stand-off distance increased, providing further evidence of the improved support from webs perpendicular to the face sheets. The severity of damage caused by the web increases as the depth of the damage becomes thicker while maintaining the same pressure. The flexural strength was primarily affected by the pressure and stand-off distance length. The longer peened size (5 mm) failed in the region between the top face sheet and the core, as illustrated in Figure 13. Compared to the shorter distance, less damage was detected on the whole skin. Remarkably, varying the pressures applied to the face sheets led to additional damage in the composite sample. This sample was constructed utilizing the identical core and materials. The strength increased due to the compactness of the material after the peening process. The strikes of the abrasive particle provided the rough and compactness.

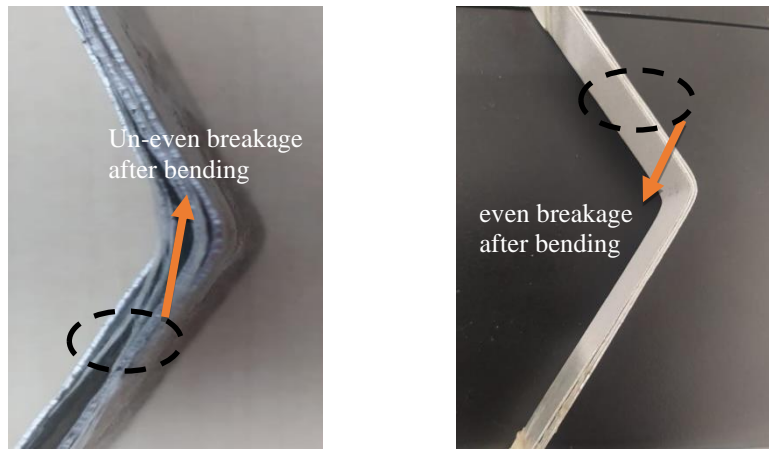


Figure 14. (a) Un-peened composite after bending test, (b) AWJP treated composite after bending test

Figure 14 shows a brittle failure mode occurring on both the top and bottom skin layers during the flexural strength testing, as can be seen in Figures 14 (a) and (b). By contrast, the coupon reinforced with glass fiber face sheets exhibited no distinct or clearly defined breakage line, indicating a different failure behavior under the same conditions. The location of the failure in the core of the bottom face sheet of the hybrid composite coupon is shown in Figure 14 (a), providing insight into the mechanical characteristics of the hybrid face sheets. Figure 14 also provides evidence of the correlation between the peening pressure of AWJP and the flexural strength of the specimens. The specimens exhibited a significant improvement in flexural strength as the peening pressure of the AWJP rose from 69 to 97 MPa.

Nevertheless, when subjected to an AWJP pressure of 97 MPa, the average flexural strength of the specimens exhibited an increase compared to the as-sintered and polished samples, which had a flexural strength of 429.1 MPa. However, the flexural strength of the specimens was lower than that of the shiny and pre-sintered samples, which had a flexural strength of 373.4 MPa. Consequently, the observed enhancement in flexural strength within the range of peening pressures from 97 to 117 MPa may be attributed to the reparative mechanism that addresses the formation of little surface fractures induced by the peening procedure.

Additionally, it is worth noting that several significant surface cracks became evident when the pressure applied during the AWJP process reached 117 MPa, as illustrated in Figure 14 (b). The loss in bending strength may be attributed to the inherent difficulty in effectively repairing extensive surface cracks. The morphological images of a composite can be seen in Figure 14 (a). These images demonstrate that the micro pits had an isotropic microstructure composed of hexagonal grains. The average grain size increased; however, minimal porosity was noted in the polished section. As illustrated in Figure 14 (b), a significant number of semi-elliptical cracks, ranging in length from 3 to 5 μm , which were observed can be seen on the surface of the bent sample following the application of AWJP at a pressure of 97 MPa.

Figure 15 provides evidence that, during nucleation, the multiplication of the attempt occurred rapidly in a direction perpendicular to the loading direction. Consequently, it was of utmost importance to address the formation of cracks that occurred during the peening process. In the case of the specimens subjected to peak pressure treatment, there was a significant decline in flexural strength, with values decreasing from 405.9 to 371.2 MPa as the AWJP pressure was elevated from 97 to 117 MPa.

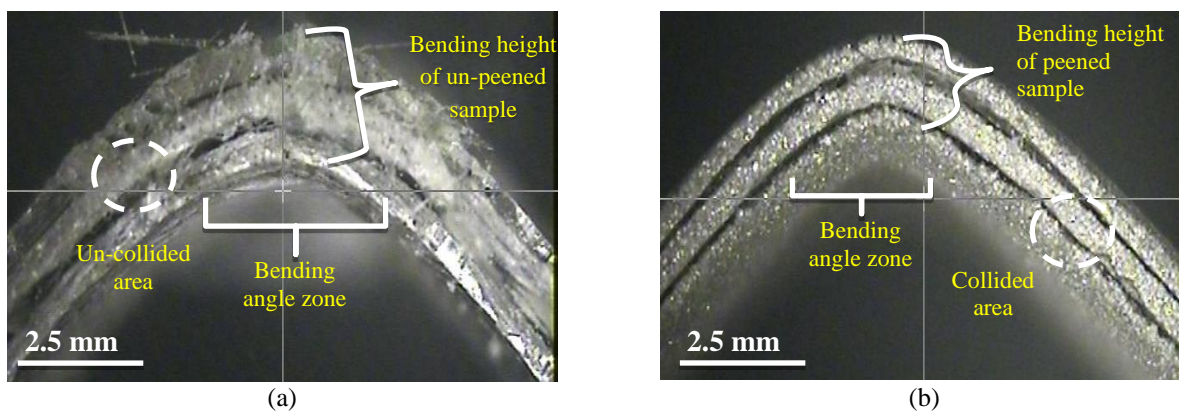


Figure 15. Fractography of the FML composite after 3-point bending test, (a) un-peened, (b) peened

The findings of this study have indicated that the application of AWJP, following crack-healing, resulted in a notable enhancement of the flexural strength of the composite material. The strength of the aluminum alloy was enhanced by applying AWJP in conjunction with single crack-healing. The current investigation revealed that the bending strengths of the specimens subjected to non-abrasive waterjet peening NAWJP and AWJP exhibited more excellent value than those

of other conditions. Figure 15 (a) and (b) provide evidence that the AWJP process would generate significant surface cracks. However, it was observed that these cracks may undergo an initial healing process through pre-oxidation. This healing mechanism led to the closure of the initial surface cracks, as can be seen in Figure 15 (a). Consequently, the damage caused by peening was reduced, and a subsequent strengthening effect was observed during the fractography study conducted as part of this research.

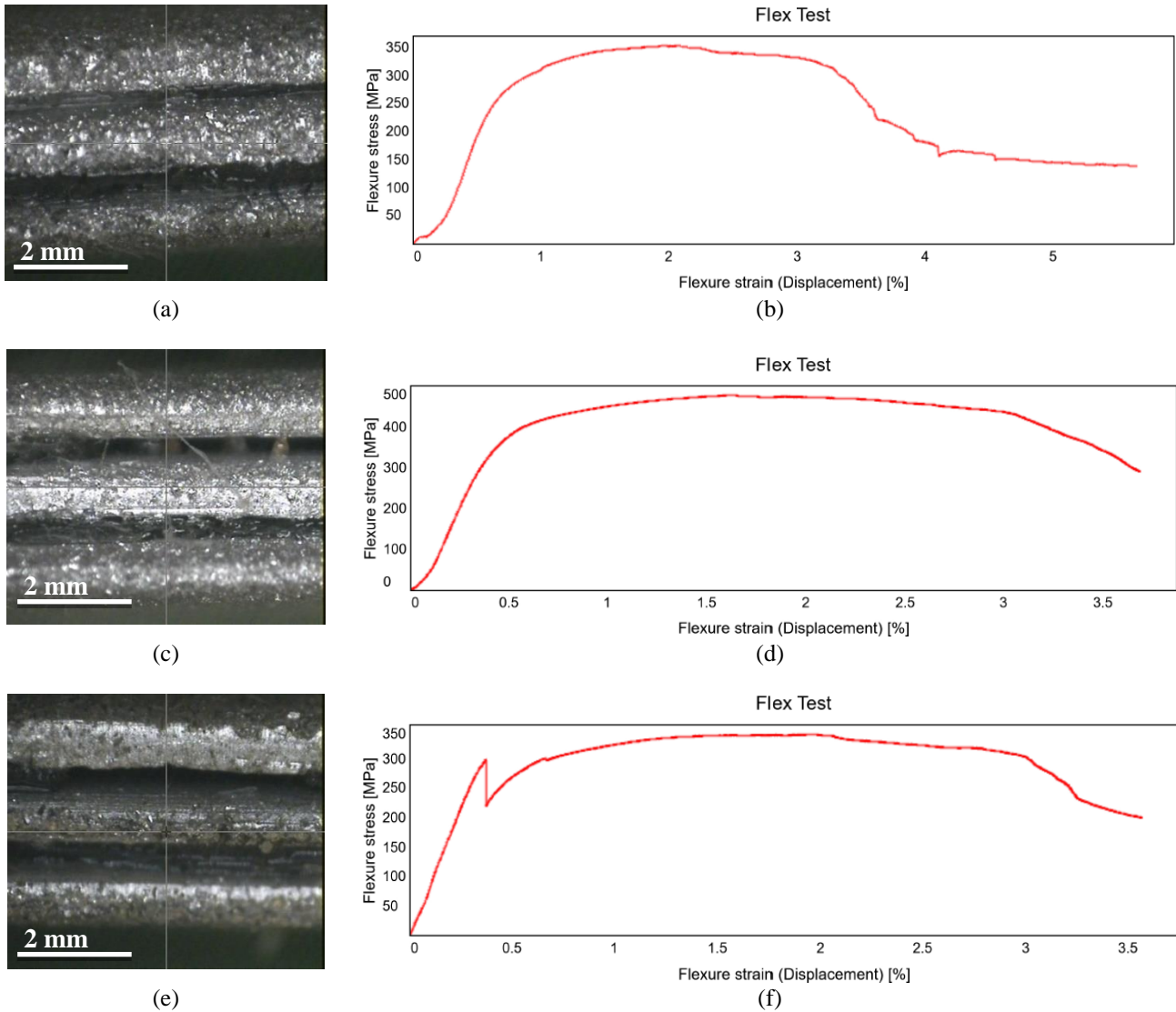


Figure 16. Influence of AWJ peening pressure at FML composite, (a) morphology of dents to 69 MPa, (b) flexural strength at 69 MPa, (c) morphology view of dents at 97 MPa, (d) flexural strength at 97 MPa, (e) surface morphology of FML composite at 117 MPa, (f) flexural strength at 117 MPa

Additionally, the simultaneous effect of produced compressive residual stresses on the surfaces of the specimens from AWJP and crack-healing contributed to the high flexural value observed, as shown in Figure 16 (a) and (b). Therefore, the utilization of AWJP in conjunction with different crack-healing techniques potentially enhanced the mechanical strength of the specimens, as can be seen in Figure 16 (c) and (d). Additionally, the findings of the present study have revealed that a pressure of 97 MPa would be the optimal value for AWJP. The fractography analysis image presented in Figures 16 (e) and (f) exhibits the microstructure of a sintered FML composite. The analysis indicated that the aluminum grains within the composite possess an isotropic nature, characterized by the presence of hexagonal grains. The average grain size was estimated to be around 2 μm , and minimal porosity was noted in the polished specimen. In Figure 16 (f), it can be seen that a significant number of semi-elliptical cracks exhibit flexural strength, indicating a low value below 350 MPa. In real-world scenarios, after initiating a fracture, it would rapidly spread in a direction perpendicular to the applied tensile load. Consequently, it is of utmost importance to address the formation of fractures occurring during the AWJP process.

Conversely, the additional pressure of 97 MPa would concern the AWJP. The observed pressure of 97 MPa was significantly higher value than that of further pressure. Furthermore, if a process continued with 97 MPa, the flexural strength value of other flexural strain percentages would be at a medium level. However, the values may fluctuate in relation to equality in the flexural strength, and interfaces between the parameters would increase the stand-off distance

and abrasive size. It was observed that the pressure of 117 MPa was significantly lower values than those of other pressures.

Furthermore, if a process continued with 117 MPa, flexural strength values with additional flexural strain percentage would deteriorate. However, in the case of fluctuating flexural strength, which would decrease the stand-off distance and abrasive size, the values would fluctuate between the parameters. It is clear from these results that the bending strength would increase proportionally to the treatment of the sample. Increasing the size of the abrasive (a) from 80 to 120 increased bending strength. The region of highest pressure, located at the center of the upper surface in contact with the specimen, displayed the most extensive damage.

4. CONCLUSIONS

In the present study, the main concern was to evaluate the resulting failure behavior of the FML before and after the surface treatment. The peening impact has been found to exhibit a higher effect on the FML bending strength due to changes in different factors. The following conclusions may be drawn from the findings of the experiment in the present study:

- The repetitive impact of the water jet onto the surface would increase the surface compactness. Moreover, it was observed that lower pressure conditions resulted in more uneven surfaces, which would benefit the surface treatment industry in preventive maintenance. Furthermore, the bending strength would positively correlate with an increase in the water supply pressure due to the heightened energy of water molecules, hence augmenting their efficacy in the material removal process.
- The previously generated craters would readily unite to form a large crater, creating consistent strength by removing all materials from the surface. AWJP was not predicted to boost bending strength for all metrics. Furthermore, related to work, AWJP specimens had lower or higher flexural strength.
- The maximal flexural strength was observed at an optimized stand-off distance, suggesting that the jet structure primarily comprised water droplets at this distance.
- As the water jet moved laterally outward, it induced surface fractures in the material through a mechanism known as pitting action. With each subsequent jet pass, pre-existing cracks would be extended further while new fractures would form. This continuous crack propagation and initiation process would enhance the material's flexural strength over time.
- Water pressure plays a vital role at the FML surface. In most cases, there was evidence of the different trend lines in the microscopy analysis. The roughness has behaved differently, mainly on the change in pressure with a combination of the other AWJP parameters.

ACKNOWLEDGEMENTS

Authors would like to gratefully acknowledge the financial support from the Ministry of Higher Education, Malaysia through FRGS/1/2019/TK03/UMPSA/02/25 and Universiti Malaysia Pahang AL-Sultan Abdullah through RDU1901161.

CONFLICT OF INTEREST

The authors declare no competing interests.

AUTHORS CONTRIBUTION

Syed Qutaba: Conceptualization, methodology, literature review, analysis and writing.

Galang Sandy: Conceptualization, methodology, collecting the data and writing—original draft.

Sajjad Ahmed: Conceptualization, paper citation, administration and drafting.

Azmir Azhari: Conceptualization, methodology, design layout, review, funding acquisition and supervision.

REFERENCES

- [1] N. Yuvaraj, M. P. Kumar, "Multiresponse optimization of abrasive water jet cutting process parameters using TOPSIS approach," *Materials and Manufacturing Processes*, vol. 30, no. 7, pp. 882–889, 2015.
- [2] A. Alberdi, A. Suárez, T. Artaza, G. A. Escobar-Palafox, K. Ridgway, "Composite cutting with abrasive water jet," *Procedia Engineering*, vol. 63, pp. 421–429, 2013.
- [3] U. Çaydaş A. Haşçalık, "A study on surface roughness in abrasive waterjet machining process using artificial neural networks and regression analysis method," *Journal of Materials Processing Technology*, vol. 202, no. 1, pp. 574–582, 2008.
- [4] P. Löschner, K. Jarosz, P. Niesłony, "Investigation of the effect of cutting speed on surface quality in abrasive water jet cutting of 316L stainless steel," *Procedia Engineering*, vol. 149, pp. 276–282, 2016.
- [5] A. Cunha, R. O. Giacomelli, J. Kaufman, J. Brajer, T. S. Pereira, "An overview on laser shock peening process: from science to industrial applications," in *2021 SBFoton International Optics and Photonics Conference (SBFoton IOPC)*, 2021, pp. 1–6.

- [6] N. Lusi, A. Fiveriati, A. Afandi, I. Gusti Ngurah Bagus Catra Wedarma, H. Yulianoko, M. Darsin, et al., "Predictive modelling on machining performance of ECDM using artificial neural network and particle swarm optimization," *Manufacturing Technology*, vol. 23, no. 5, pp. 649–662, 2023.
- [7] S. L. Yao, G. Y. Wang, H. Yu, J. Wang, K. S. Li, S. Liu et al., "Influence of submerged micro-abrasive waterjet peening on surface integrity and fatigue performance of TA19 titanium alloy," *International Journal of Fatigue*, vol. 164, p. 107076, 2022.
- [8] S. Yao, G. Wang, K. Li, N. Wang, C. Zhang, S. Liu et al., "Cavitation abrasive integrated waterjet peening process and the effect of process parameters on the surface integrity of TA19 titanium alloy," *Surface and Coatings Technology*, vol. 440, p. 128477, 2022.
- [9] L. D. Minh, N. Q. Sang, P. Bilik, R. Martinek, "Optimized design of source energy for manufacturing machine by digital numerical control," *International Journal of Automotive and Mechanical Engineering*, vol. 20, no. 1 SE-Articles, pp. 10307–10321, 2023.
- [10] D. Arola, A. E. Alade, W. Weber, "Improving fatigue strength of metals using abrasive waterjet peening," *Machining Science and Technology*, vol. 10, no. 2, pp. 197–218, 2006.
- [11] Z. Wang, Z. Liao, D. Axinte, X. Dong, D. Xu, G. Augustinavicius, "Analytical model for predicting residual stresses in abrasive waterjet peening," *Materials & Design*, vol. 212, p. 110209, 2021.
- [12] X. Miao, T. Long, M. Wu, C. Ma, Q. Wang, "Study on the process of abrasive water jet peening for 316L stainless steel," *International Journal of Advanced Manufacturing Technology*, vol. 120, no. 11, pp. 8321–8328, 2022.
- [13] P. Chandrasekaran, S. Ashok, R. Ajaykumar, N. Ashokkumar, R. Sathya, S. Karpagavalli et al., "Application of defoliants alters leaf growth and gas exchange parameters for cotton defoliation," *Plant Science Today*, vol. 10, no. 4, pp. 105–114, 2023.
- [14] Y. Natarajan, P. K. Murugesan, M. Mohan, S. A. Liyakath Ali Khan, "Abrasive water jet machining process: A state of art of review," *Journal of Manufacturing Processes*, vol. 49, pp. 271–322, 2020.
- [15] P. Zhang, X. Yue, P. Wang, Y. Zhai, "Influence of SiC pellets water jet peening on the surface integrity of 7075-T6 aluminum alloy," *Vacuum*, vol. 196, p. 110760, 2022.
- [16] S. Karthik, H. J. Amarendra, "Slurry jet erosion test rig: A review of erosive particles induction methods and its test parameters," *Journal of Bio-and Tribo-Corrosion*, vol. 6, no. 3, p. 101, 2020.
- [17] M. Palleda, "A study of taper angles and material removal rates of drilled holes in the abrasive water jet machining process," *Journal of Materials Processing Technology*, vol. 189, no. 1, pp. 292–295, 2007.
- [18] G. Aydin, I. Karakurt, K. Aydiner, "An investigation on surface roughness of granite machined by abrasive waterjet," *Bulletin of Materials Science*, vol. 34, no. 4, pp. 985–992, 2011.
- [19] S. Qutaba, M. Asmelash, K. Saptaji, A. Azhari, "A review on peening processes and its effect on surfaces," *International Journal of Advanced Manufacturing Technology*, vol. 120, no. 7–8, pp. 4233–4270, 2022.
- [20] S. Qutaba, M. Asmelash, A. Azhari, "Effect of surface topography of 8090 Al-Li alloy during abrasive waterjet peening process," in *AIP Conference Proceedings*, vol. 2998, no. 1, p. 060005, 2024.
- [21] H. Soyama, D. Sanders, "Use of an Abrasive Water Cavitating Jet and Peening Process to Improve the Fatigue Strength of Titanium Alloy 6Al-4V Manufactured by the Electron Beam Powder Bed Melting (EBPB) Additive Manufacturing Method," *JOM*, vol. 71, no. 12, pp. 4311–4318, 2019.
- [22] X. Li, X. Zhang, Y. Guo, V. P. W. Shim, J. Yang, G. B. Chai, "Influence of fiber type on the impact response of titanium-based fiber-metal laminates," *International Journal of Impact Engineering*, vol. 114, pp. 32–42, 2018.
- [23] X. Li, X. Zhang, H. Zhang, J. Yang, A. B. Nia, G. B. Chai, "Mechanical behaviors of Ti/CFRP/Ti laminates with different surface treatments of titanium sheets," *Composite Structures*, vol. 163, pp. 21–31, 2017.
- [24] N. Mokhtar, S. Qutaba, M. Asmelash, M. A. Azhari, "Impact of pressure on surface roughness and kerf characteristics using low pressure abrasive water jet cutting," *Surface Engineering and Applied Electrochemistry*, vol. 60, no. 1, pp. 129–141, 2024.
- [25] C. Russig, M. Bambach, G. Hirt, N. Holtmann, "Shot peen forming of fiber metal laminates on the example of GLARE®," *International Journal of Material Forming*, vol. 7, no. 4, pp. 425–438, 2014.
- [26] H. Li, Y. Lu, J. Xiang, Z. Han, X. Xu, H. Wang et al., "Residual stresses and failure behavior of GFRP/Al-Li laminates after single and multiple shot's indentation under quasi-static," *Composites Part A: Applied Science and Manufacturing*, vol. 130, p. 105761, 2020.
- [27] K. M. Subbaya, K. Nithin, S. Sachhidananda, "Fiber reinforced composites-a review," *Journal of Material Sciences & Engineering*, vol. 6, no. 03, pp. 2–6, 2017.
- [28] A. Purnowidodo, S. Sofyan Arief, F. Hilmi Iman, "Effect surface roughness on fatigue crack propagation behaviour of fibre metal laminates (FMLs)," *International Journal of Automotive and Mechanical Engineering*, vol. 16, no. 2 SE-Articles, pp. 6588–6604, 2019.
- [29] R. A. Pethrick, "Composite to metal bonding in aerospace and other applications," in *Woodhead Publishing Series in Welding and Other Joining Technologies*, pp. 288–319, 2012.
- [30] K. Bousnina, A. Hamza, N. Ben Yahia, "Energy optimization for milling 304L steel using artificial intelligence methods," *International Journal of Automotive and Mechanical Engineering*, vol. 19, no. 3, pp. 9928–9938, 2022.
- [31] S. M. Luz, A. R. Gonçalves, A. P. Del'Arco, "Mechanical behavior and microstructural analysis of sugarcane bagasse fibers reinforced polypropylene composites," *Composites Part A: Applied Science and Manufacturing*, vol. 38, no. 6, pp. 1455–1461, 2007.

- [32] S. Ahmed, "Emergent technologies in human detection for disaster response: A critical review," *Sukkur IBA Journal of Emerging Technologies*, vol. 7, no. 1, pp. 56–78, 2024.
- [33] Z. A. Abro, C. Hong, Y. Zhang, M. Q. Siddiqui, A. M. R. Abbasi, Z. Abro et al., "Development of FBG pressure sensors using FDM technique for monitoring sleeping postures," *Sensors and Actuators A: Physical*, vol. 331, p. 112921, 2021.
- [34] L. C. Thomas, V. Kumar, A. Gangwar, M. Pisupati, C. Gupta, and S. K. Panda, "Computational modelling and experimental techniques for fibre metal laminate structural analysis: A comprehensive review," *Archives of Computational Methods in Engineering*, vol. 31, no. 1, pp. 351–369, 2024.
- [35] M. A. Azmir and A. K. Ahsan, "A study of abrasive water jet machining process on glass/epoxy composite laminate," *Journal of Materials Processing Technology*, vol. 209, no. 20, pp. 6168–6173, 2009.
- [36] A. K. Dahiya, B. K. Bhuyan, and S. Kumar, "Perspective study of abrasive water jet machining of composites—A review," *Journal of Mechanical Science and Technology*, vol. 36, no. 1, pp. 213–224, 2022.
- [37] S. Qutaba, M. Asmelash, and A. Azhari, "Investigation on the multiple plies structure of aluminum-lithium alloy and glass fiber composite with respect to deformation failure," *Materials Research Express*, vol. 10, no. 1, p. 016507, 2023.
- [38] S. Sugiman, A. D. Crocombe, K. B. Katnam, "Investigating the static response of hybrid fibre–metal laminate doublers loaded in tension," *Composites Part B: Engineering*, vol. 42, no. 7, pp. 1867–1884, 2011.
- [39] M. S. Fadly, A. Purnowidodo, P. H. Setyarini, B. Bakri, S. Chandrabakty, "Experimental and numerical modelling of ballistic impact on fiber metal laminates based on aramid fiber reinforced epoxy," *International Journal of Automotive and Mechanical Engineering*, vol. 21, no. 3, pp. 11554–11568, 2024.
- [40] S. Qutaba, A. Azhari, M. Asmelash, M. Haider, N. Lusi, "Development of fiber metal laminate composite with different glass fiber GSM," *Materials Today: Proceedings*, vol. 107, pp. 120–127, 2023.
- [41] D. Quan, G. Wang, G. Zhao, R. Alderliesten, "On the fracture behaviour of aerospace-grade Polyether-ether-ketone composite-to-aluminium adhesive joints," *Composites Communications*, vol. 30, p. 101098, 2022.
- [42] M. Bagci, "Influence of fiber orientation on solid particle erosion of uni/multidirectional carbon fiber/glass fiber reinforced epoxy composites," *Proceedings of the Institution of Mechanical Engineers, Part J: Journal of Engineering Tribology*, vol. 231, no. 5, pp. 594–603, 2017.
- [43] Z. Ding, H. Wang, J. Luo, N. Li, "A review on forming technologies of fibre metal laminates," *International Journal of Lightweight Materials and Manufacture*, vol. 4, no. 1, pp. 110–126, 2021.
- [44] A. Ravindra, E. S. Dwarakadasa, T. S. Srivatsan, C. Ramanath, K. V. V. Iyengar, "Electron-beam weld microstructures and properties of aluminium-lithium alloy 8090," *Journal of Materials Science*, vol. 28, no. 12, pp. 3173–3182, 1993.
- [45] R. J. H. Wanhill, "Status and prospects for aluminium-lithium alloys in aircraft structures," *International Journal of Fatigue*, vol. 16, no. 1, pp. 3–20, 1994.
- [46] B. Han, W. Tao, Y. Chen, H. Li, "Double-sided laser beam welded T-joints for aluminum-lithium alloy aircraft fuselage panels: Effects of filler elements on microstructure and mechanical properties," *Optics & Laser Technology*, vol. 93, pp. 99–108, 2017.
- [47] A. Iqbal, N. U. Dar, G. Hussain, "Optimization of abrasive water jet cutting of ductile materials," *Journal of Wuhan University of Technology-Materials Science Edition*, vol. 26, no. 1, pp. 88–92, 2011.